Appl. Phys. A 88, 769–773 (2007)
DOI: 10.1007/s00339-007-4078-6

Applied Physics A
Materials Science & Processing

H.W. KIM✉
S.H. SHIM

Temperature-controlled fabrication of SnO_2 nanoparticles via thermal heating of Sn powders

School of Materials Science and Engineering, Inha University, Incheon 402-751, Republic of Korea

Received: 13 November 2006 / Accepted: 17 April 2007
Published online: 20 June 2007 • © Springer-Verlag 2007

ABSTRACT We report a method by which we have produced nano-sized crystalline tin oxide (SnO_2) particles with a rutile structure. We have employed thermal evaporation of solid Sn powders in ambient air. Samples were characterized by scanning electron microscopy, X-ray powder diffraction, transmission electron microscopy, and photoluminescence (PL) spectroscopy. The size of SnO_2 particles in an agglomerated state was found to decrease on decreasing the synthesis temperature in the range of 700–850 °C. The product synthesized at a low temperature of 700 °C was comprised of a trace amount of tetragonal SnO phase. Photoluminescence spectra showed visible light emission, with its overall intensity being increased on increasing the synthesis temperature.

PACS 81.07.Wx; 81.05.Hd; 61.10.Nz; 68.37.Hk; 68.37.Lp

1 Introduction

The synthesis of nanosized particles has attracted considerable interest in the various fields of chemistry, physics, and materials science, due to their novel physicochemical properties differing significantly from macroscopic phases [1–3]. With the decrease of the crystal size, the large interfacial areas, homogeneity and highly reactive surfaces of the nanocrystalline particles and other useful properties have attracted much attention. In particular, semiconductor nanoparticles have been extensively studied from both experimental and theoretical viewpoints. Among them, tin oxide (SnO_2) is a prototypical optically transparent n-type semiconductor with a wide band gap ($E_g = 3.62$ eV at 300 K), which spans a wide range of applications such as resistors, gas sensors, special coatings for energy-conserving "low-emissivity" windows, transparent heating elements, electrodes in glass melting furnaces, antistatic coatings, and optoelectronic devices [4–9]. In recent years, considerable efforts have been focused on the synthesis of SnO_2 nanostructured thin films [10–14], nanowires, nanotubes, and nanoparticles, with the exploration of their novel properties. In particular, a variety of methods, such as sol–gel [15], pulsed laser

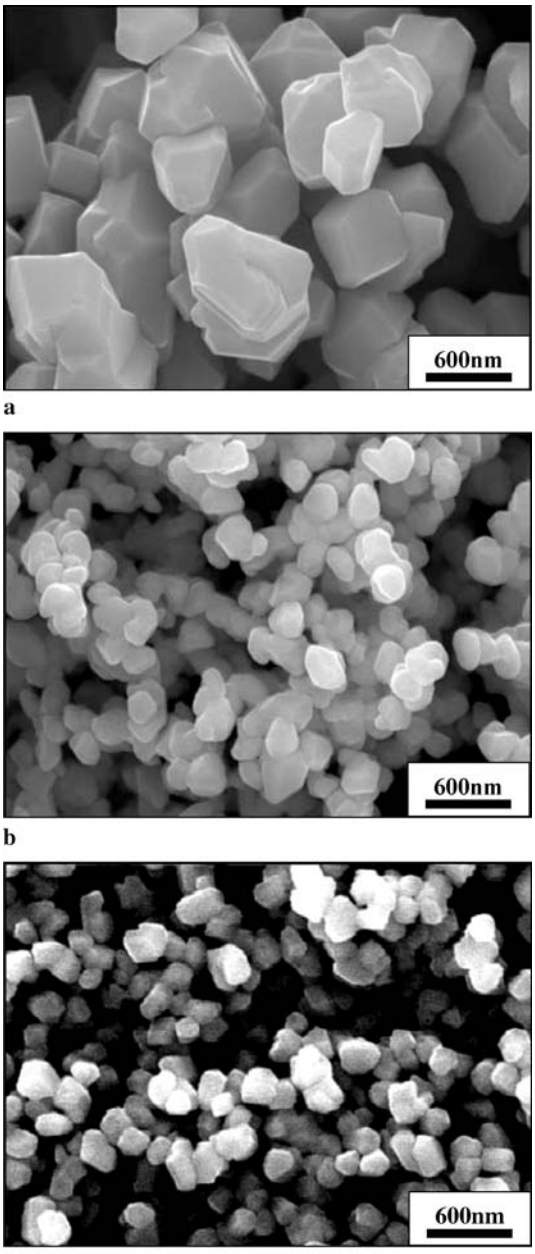

FIGURE 1 SEM image of the products synthesized at (**a**) 850 °C, (**b**) 780 °C, and (**c**) 700 °C

✉ Fax: +82-32-860-7544, E-mail: hwkim@inha.ac.kr

deposition [16], mechanochemical [17] and wet-chemical synthesis [18–22] have been used to produce SnO_2 nanoparticles. Since consideration of the simplicity and affordability of a method still remains a challenge for the scientist involved in the development of new synthetic routes, in the present paper, we have demonstrated the synthesis of crystalline SnO_2 nanoparticles by a simple and low-cost thermal evaporation of Sn powders, which ensures a potential application to commercial VLSI devices and systems [23–25]. Here we report investigations into the changes in morphology and other properties by varying the growth temperature. We were particularly interested in controlling the particle size, because the physical properties of a nanodimensional material depends on its particle size. In addition, we investigated their structural and photoluminescence (PL) characteristics.

2 Experimental

The synthesis process was carried out in a quartz tube (diameter: 55 mm). The source material was pure Sn powder. We employed iridium (Ir: about 150 nm)-coated Si substrates. On top of the alumina boat with the source material, a piece of the substrate was placed with the deposition side downwards. The vertical distance between the alumina boat and the substrate was approximately 10 mm. The quartz tube was inserted into a horizontal tube furnace. During the experiment, the furnace was kept at a constant total pressure of 1 Torr with the ambient gas ($Ar + O_2$) gas. The typical percentage of O_2 and Ar partial pressures were set to approximately 3 and 97%, respectively. Previous experiments indicated that no SnO_2 has been deposited at temperatures below 650 °C. For a comparison study, the synthesis temperatures were set to 700 °C, 780 °C, and 850 °C. When the system was cooled down to room temperature after 2 h of typical deposition, the substrate was removed from the furnace for further characterization.

The as-grown samples were characterized and analyzed by using glancing-angle X-ray diffraction (XRD, Philips

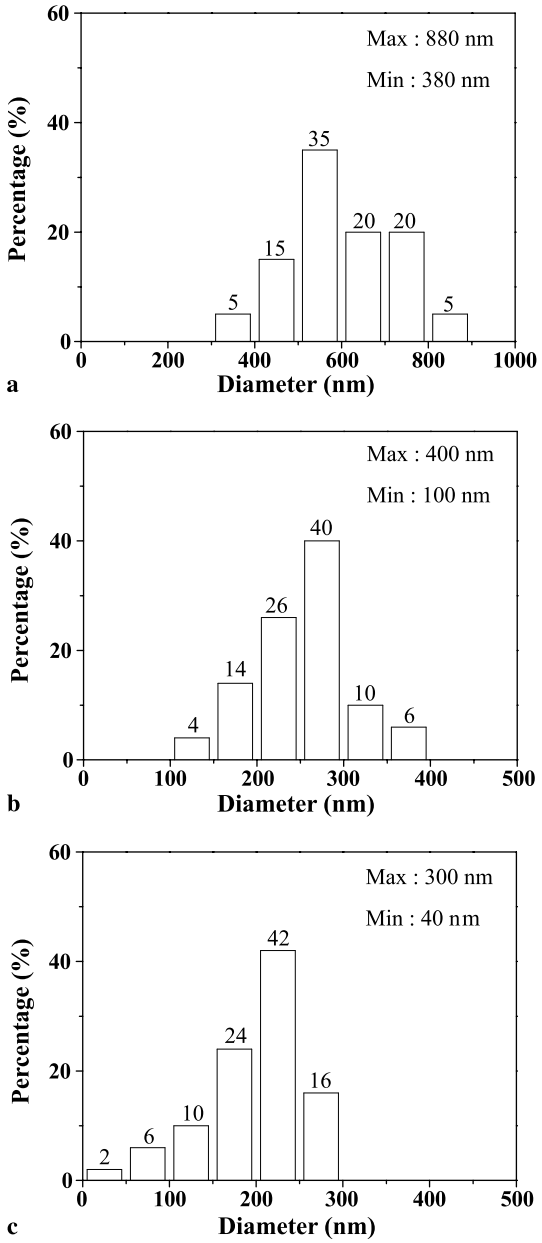

FIGURE 2 The diameter distribution of the products synthesized at (**a**) 850 °C, (**b**) 780 °C, and (**c**) 700 °C

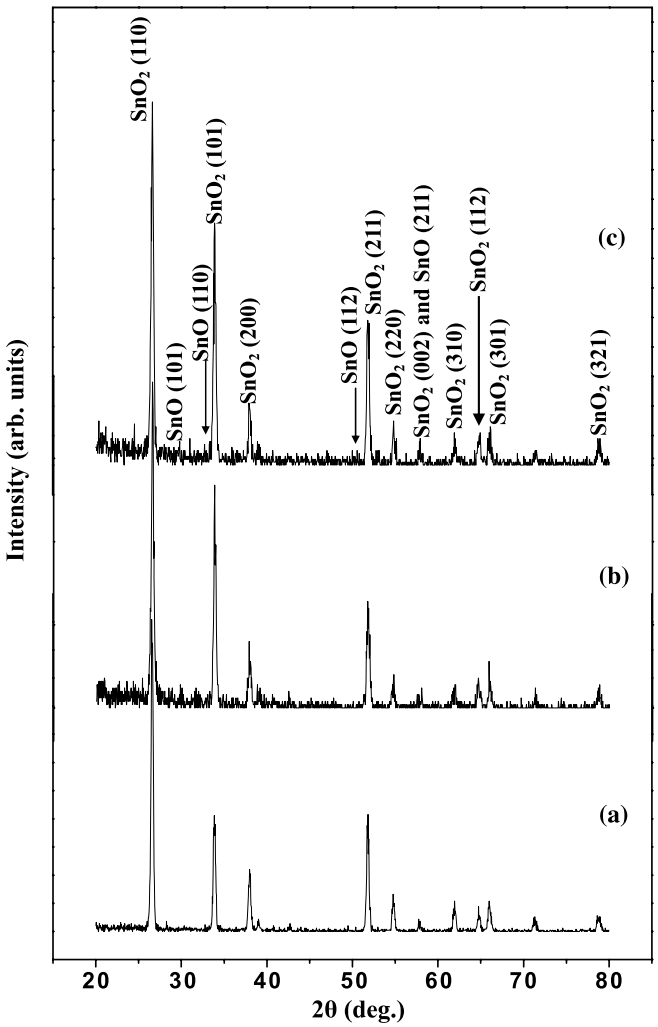

FIGURE 3 XRD pattern of the product synthesized at (**a**) 850 °C, (**b**) 780 °C, and (**c**) 700 °C

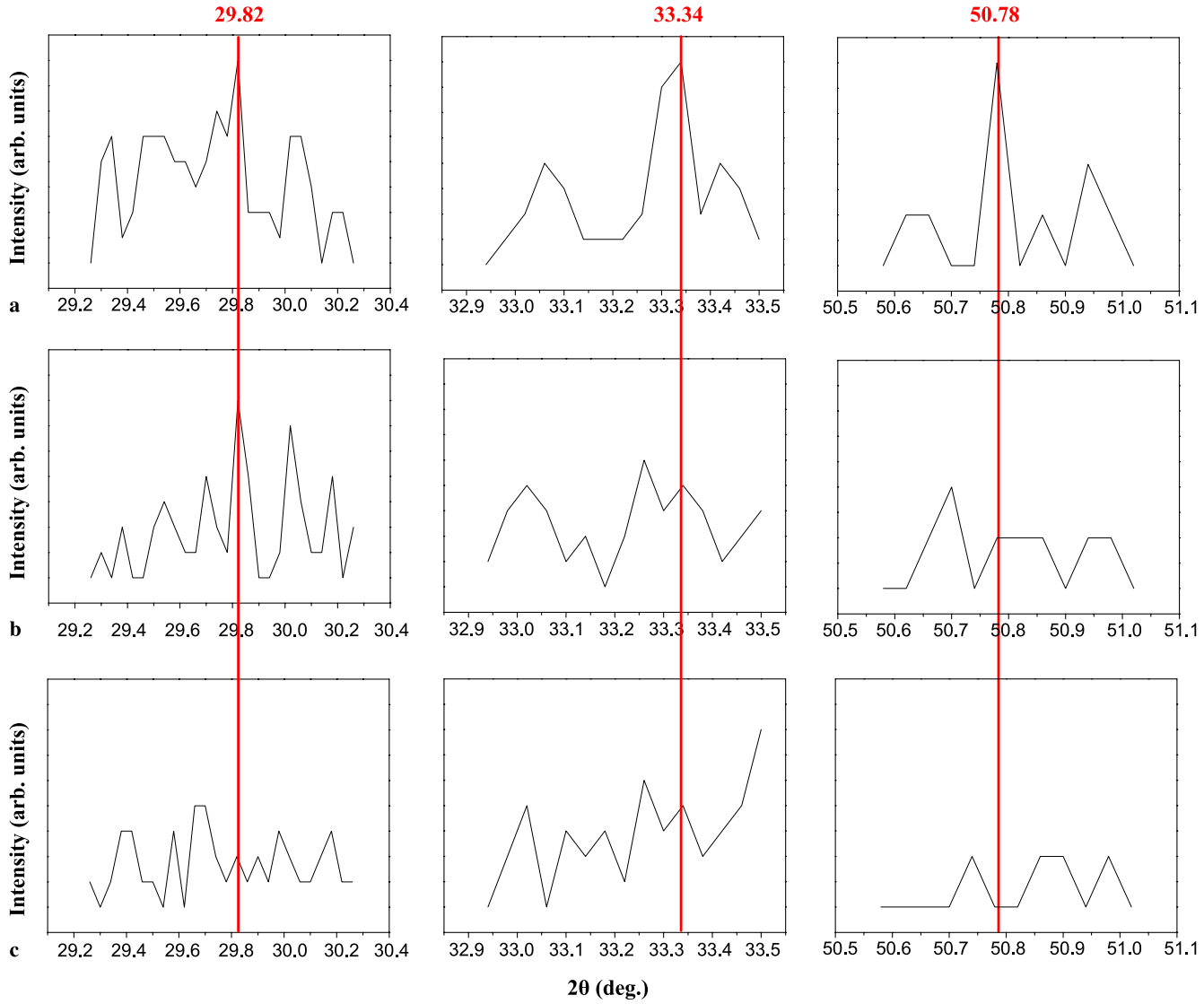

FIGURE 4 Enlarged view of the XRD spectrum with the 2θ values in the range of 29.3–30.2°, 33.0–33.5°, and 50.6–51.0°, from the samples synthesized at (**a**) 850 °C, (**b**) 780 °C, and (**c**) 700 °C

X'pert MRD) with an incidence angle of 0.5°, scanning electron microscopy (SEM, Hitachi S-4200), and transmission electron microscopy (TEM, Philips CM-200). For the TEM observation, the products were ultrasonically dispersed in acetone, and a drop of the solution was placed on a Cu grid coated with a porous carbon film. Photoluminescence measurements were performed by using a He-Cd laser line (325 nm, 55 mW) as the excitation source at 298 K.

3 Results and discussion

Typical top-view SEM images of the samples with synthesis temperatures of 850 °C, 780 °C, and 700 °C, respectively, are shown in Fig. 1a–c. The products mainly consist of particles in an agglomerated state, regardless of the temperature during the synthetic process. Close examination of Fig. 1a reveals that most particles produced at 850 °C are nearly polyhedron-shaped with some facets. Statistical analysis of many SEM images indicates that the diameter of particles with the growth temperature of 700 °C, 780 °C, and 850 °C, respectively, are in the range of 40–300 nm, 100–400 nm, and 380–880 nm. These results indicate that the average diameter of particles overall increases with increasing the temperature in the range of 700–850 °C. For clarity, the diameter distributions of the particles are displayed in Fig. 2. They reveal that the maxima of diameter distributions occur in range of 250–300 nm and 200–250 nm, respectively, for the products synthesized at 780 °C and 700 °C.

The XRD patterns recorded from the samples synthesized at 850 °C, 780 °C, and 700 °C are shown in Fig. 3a–c, respectively. The diffraction peaks of the (110), (101), (200), (211), (220), (002), (310), (112), (301) and (321) planes can be indexed based on a tetragonal cell with cell parameters $a = 4.734$ Å and $c = 3.185$ Å, which is in good agreement with the known data (JCPDS No. 41-1445). For the sample synthesized at 700 °C (Fig. 3c), it is noteworthy that peaks at around 29.82°, 33.34°, 50.78°, and 57.40° can be indexed to the (101), (110), (112), and (211) reflection of the tetragonal structure of SnO with lattice constants of $a = 3.802$ Å and $c = 4.836$ Å (JCPDS File No. 06-0395). Since the existence

of those peaks is not clear from Fig. 3a and b, we have presented an enlarged view of the XRD spectra with the 2θ values in the range of 29.3–30.2°, 33.0–33.5°, and 50.6–51.0°, as shown in Fig. 4. Figure 4a–c show the enlarged XRD spectra with respect to the samples synthesized at 850 °C, 780 °C, and 700 °C, respectively. Close examination indicated that the XRD spectra of the 700 °C-synthesized sample clearly exhibited the peaks at around 29.82°, 33.34°, and 50.78°, whereas the XRD spectra of the 850 °C-synthesized sample did not clearly show those peaks. Also, although XRD spectra of the 780 °C-synthesized sample exhibited the peak at around 29.82°, no clear peak was found at around 33.34° and 50.78°. To summarize, we reveal that the products mainly consist of tetragonal SnO_2 phase, regardless of synthesis temperature in the range of 700–850 °C. In addition, the 700 °C-synthesized sample is comprised of a trace amount of tetragonal SnO phase, whereas the 850 °C-synthesized sample does not show strong evidence for the existence of SnO phase. We suggest that the amount of SnO phase increases with increasing the synthesis temperature in the range of 700–850 °C. Pure liquid Sn is known to oxidize rapidly especially at 700–800 °C [26]. It is generally agreed that SnO, which forms at the initial stage of oxidation of Sn, is metastable and decomposes according to the reaction: $2SnO = SnO_2 + Sn$ [26–29]. Moreover, the higher the reaction temperature the faster is the rate of phase transformation from SnO to SnO_2. Accordingly, we surmise that the reduction of the SnO phase at a synthesis temperature of 850 °C is associated with the phase transformation of SnO to SnO_2.

Typical low magnification TEM images of produced nanoparticles are shown in Figs. 5a–d. We found a particle which is polyhedron-shaped with some facets (Fig. 5a) and a particle with a shape close to spherical (Fig. 5b). Moreover, we also observed irregularly-shaped particles (Figs. 5c and 5d). Representative high resolution TEM (HRTEM) image enlargement a part of the particle in Fig. 5c is given in Fig. 5e. Lattice fringes are clearly visible from the HRTEM image, revealing its single crystalline nature. The interplanar spacings are about 0.32 nm and 0.33 nm, respectively, corresponding to the (001) and (110) planes of the rutile tetragonal SnO_2. The associated selected area electron diffraction (SAED) pattern is shown in the inset of Fig. 5e, which can be indexed as a tetragonal rutile SnO_2 single crystal, in good agreement with the XRD results presented above. It is known that the representative high-symmetry structure of the rutile SnO_2 corresponds to a polyhedron which is formed by a Sn atom in the center, surrounded by six O atoms in the vertex. In the present study, polyhedron-shaped and spherical-shaped particles coexist in the product and even the spherical-shaped particles are close to pseudo-polyhedral structures (Fig. 5b). The irregular-shaped nanoparticles may correspond to an intermediate case. Usually, the polyhedral lattice space symmetry can be lowered by the various defects including vacant lattice site, vacancy cluster, and local disorder which cause lattice distortion [10]. However, in the present work, the quasi-spherical-shaped nanoparticles were also crystalline SnO_2 structures. Therefore, we surmise that there is a competition between two tendencies; to grow into the polyhedron-shaped structures with the extension of polyhedral lattice space symmetry and to grow into the spherical-shaped structures to reduce the surface energy of particles. Further study is underway.

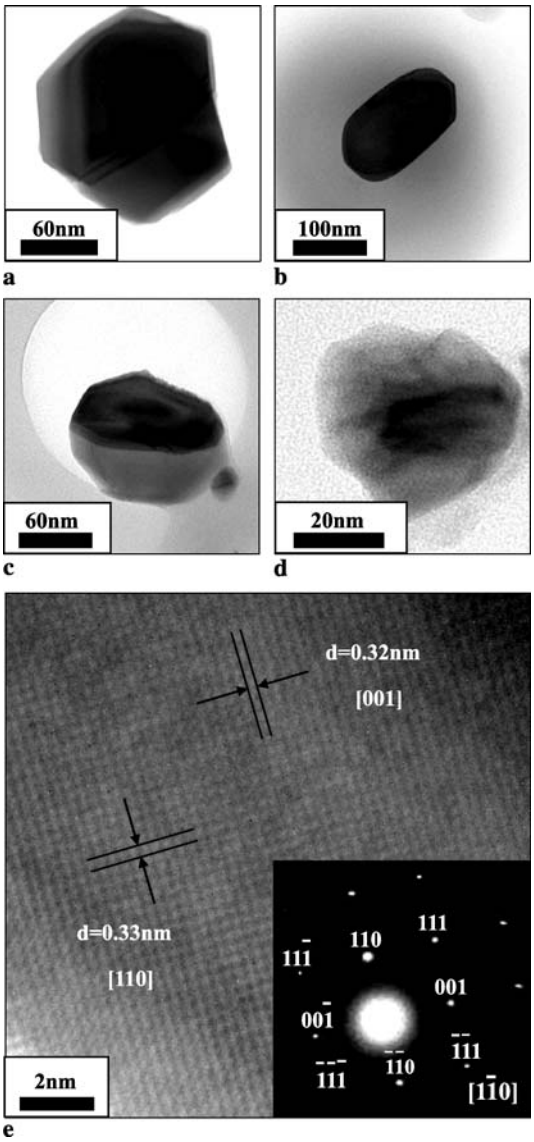

FIGURE 5 (**a**)–(**d**) TEM images of the particles. (**e**) HRTEM image corresponding to an area in (**c**) (*Inset*: corresponding SAED pattern)

It can be observed that the average particle diameter increased on increasing the growth temperature (Fig. 1). One possibility is that higher temperatures may increase the rate of supply of Sn atoms from the evaporation source (i.e. Sn powders). The other possibility may lie in the expectation that the higher reaction temperature enables a faster phase transformation from gaseous SnO to solid SnO_2. We surmise that both phenomena may contribute to further formation and growth of atom clusters, ultimately resulting in the generation of bigger SnO_2 particles. In addition, high temperature processing may facilitate in-situ sintering or annealing, presumably resulting in the coalescence of particles on the substrate surface. The small particles may join-up with the neighbouring particles, reducing the surface energy. Accordingly, although more investigation is necessary to reveal the detailed mechanism, it is clear from our result that different sized particles can be prepared by controlled heating.

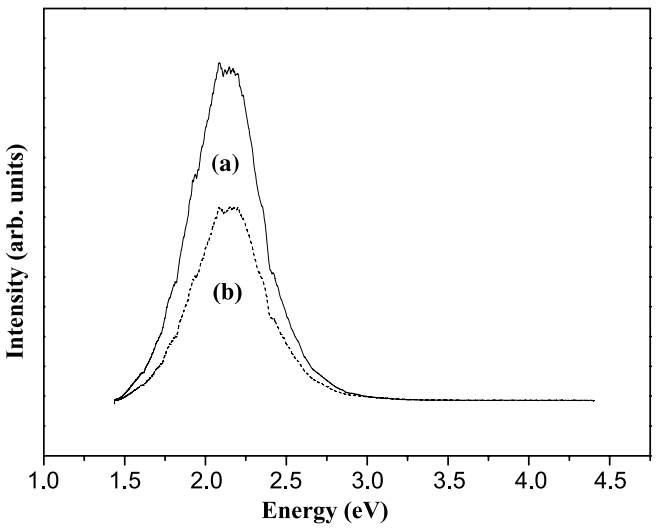

FIGURE 6 PL spectrum of the products synthesized at (a) 850 °C and (b) 700 °C with a photoexcitation energy of 3.82 eV

Photoluminescence spectra of 850 °C-synthesized and 700 °C-synthesized samples are shown in 6 a and b. The reported band gap of SnO_2 is an indirect band gap of 3.6 eV [30]. Therefore, an excitation energy of the He-Cd laser ($\lambda_{ex} = 325\,nm = 3.82\,eV$) would be high enough to pump carriers to the excited states. The dominant emissions from all two samples are bands that peaked at an energy of around 2.09–2.14 eV, corresponding to the wavelength of about 581–595 nm in the yellow region. Previous researchers have reported yellow emission [31, 32] from SnO_2 structures. Yellow luminescence is known to be associated with defect energy levels within the band gap of SnO_2, being associated with O vacancies or Sn interstitials that have formed during the synthesis process [31, 32]. Although there is a similarity in the shape of PL spectra for two samples, we reveal that the overall emission intensity becomes stronger on increasing the synthesis temperature. We surmise that the increased amount of defects such as O vacancies or Sn interstitials in a higher-temperature process helps to increase the PL emission intensity.

4 Conclusions

In summary, we have prepared SnO_2 particles by thermal evaporation of Sn powders in ambient air flow. Structural and morphological characterization indicates that the as-synthesized particles were agglomerated in nature. The size of SnO_2 particles decreases on reducing the synthesis temperatures in the range of 700–850 °C. The particles are mainly composed of a crystalline SnO_2 tetragonal rutile structure. The 700 °C-synthesized sample comprises a trace amount of SnO structure. Optical measurements show that the SnO_2 particles generate a visible light emission that may be exploited in optoelectronic devices. The 850 °C-synthesized sample exhibits the higher PL emission intensity than the 700 °C-synthesized sample.

ACKNOWLEDGEMENTS This work was supported by an INHA University research grant.

REFERENCES

1 K. Suenaga, C. Colliex, N. Demoncy, A. Loiseau, H. Pascard, F. Willaime, Science **278**, 653 (1997)
2 S. Sun, C.B. Murray, D. Weller, L. Folks, A. Moser, Science **287**, 1089 (2000)
3 W.-S. Liao, T. Yang, E.T. Castellana, S. Kataoka, P.S. Cremer, Adv. Mater. **18**, 2240 (2006)
4 A. Aoki, H. Sasakura, Japan. J. Appl. Phys. **9**, 582 (1970)
5 C. Tatsuyama, S. Ichimura, Japan. J. Appl. Phys. **15**, 843 (1976)
6 E.R. Leite, I.T. Weber, E. Longo, J.A. Varela, Adv. Mater. **12**, 965 (2000)
7 R.C. Aiyer, S.G. Ansari, P. Boroojerdian, R.N. Karekar, S.K. Kulkarni, S.R. Sainkar, Thin Solid Films **295**, 271 (1997)
8 C. Nayral, E. Viala, V. Colliere, P. Fau, F. Senocq, A. Maisonnat, B. Chaudret, Appl. Surf. Sci. **164**, 219 (2000)
9 W.P. Tai, J.-H. Oh, Thin Solid Films **422**, 220 (2002)
10 Z.W. Chen, J.K.L. Lai, C.H. Shek, Phys. Rev. B **70**, 165 314 (2004)
11 Z.W. Chen, J.K.L. Lai, C.H. Shek, H.D. Chen, J. Mater. Res. **18**, 1289 (2003)
12 Z.W. Chen, J.K.L. Lai, C.H. Shek, H.D. Chen, Appl. Phys. A **81**, 1073 (2005)
13 Z.W. Chen, J.K.L. Lai, C.H. Shek, J. Solid State Chem. **178**, 892 (2005)
14 Z.W. Chen, J.K.L. Lai, C.H. Shek, Appl. Phys. Lett. **89**, 231 902 (2006)
15 F. Gu, S.F. Wang, M.K. Lü, G.J. Zhou, D. Xu, D.R. Yuan, J. Phys. Chem. B **108**, 8119 (2004)
16 Z.W. Chen, J.K.L. Lai, C.H. Shek, H.D. Chen, Appl. Phys. A **81**, 959 (2005)
17 L.M. Cukrov, T. Tsuzuki, P.G. McCormick, Script. Mater. **44**, 1787 (2001)
18 J.J. Zhu, Z.H. Lu, S.T. Aruna, D. Aurbach, A. Gedanken, Chem. Mater. **12**, 2557 (2000)
19 M. Ocana, C.J. Serna, E. Matijevi, Mater. Lett. **12**, 32 (1991)
20 Y. He, Y. Li, J. Yu, Y. Qian, Mater. Lett. **40**, 23 (1999)
21 H.-J. Ahn, H.-C. Choi, K.-W. Park, S.-B. Kim, Y.-E. Sung, J. Phys. Chem. B **108**, 9815 (2004)
22 T. Nütz, M. Haase, J. Phys. Chem. B **104**, 8430 (2000)
23 K.-M. Lee, D.-J. Lee, H. Ahn, Mater. Lett. **58**, 3122 (2004)
24 V.M. Jimenez, A.R. Gonzalez-Elipe, J.P. Espinos, A. Justo, A. Fernandez, Sens. Actuators B **31**, 29 (1996)
25 V.M. Jimenez, A. Caballero, A. Fernandez, J.P. Espinos, M. Ocana, A.R. Gonzalez-Elipe, Solid State Ionics **116**, 117 (1999)
26 D.-W. Yuan, R.-F. Yan, G. Simkovich, J. Mater. Sci. **34**, 2911 (1999)
27 J.G. Nover, F.D. Richardson, Trans. Inst. Min. Met. **81**, 63 (1972)
28 Z.R. Dai, Z.W. Pan, Z.L. Wang, Adv. Funct. Mater. **13**, 9 (2003)
29 J.Q. Hu, X.L. Ma, N.G. Shang, Z.Y. Xie, N.B. Wong, C.S. Lee, S.T. Lee, J. Phys. Chem. B **106**, 3823 (2002)
30 T.L. Credelle, C.G. Fonstad, R.H. Rediker, Bull. Am. Phys. Soc. **16**, 519 (1971)
31 J.Q. Hu, Y. Bando, Q. Liu, D. Golberg, Adv. Funct. Mater. **13**, 493 (2003)
32 B. Cheng, J.M. Russell, W. Shi, L. Zhang, E.T. Samulski, J. Am. Chem. Soc. **126**, 5972 (2004)